Supporting Information

Adsorption of Zn(II) on Amination@Wood-Aerogel and high-value reuse to ZnO/ZnS as efficient photocatalyst

Wanqi Zhang[a, †], Lili Li[a, †], Xiaotao Zhang[b,c, †,*], Hui Liu[a], Yuhong An[a], Yuan Zhong[a], Zichu Hu[b], Xiaofei Shan[a], Jing Wu[a], Marshall White[d], Zhangjing Chen[d], Ximing Wang[a,c,*]

[a] College of Material Science and Art Design, Inner Mongolia Agricultural University, Hohhot 010018, China.

[b] College of Science, Inner Mongolia Agricultural University, Hohhot 010018, China.

[c] Inner Mongolia Key Laboratory of Sandy Shrubs Fibrosis and Energy Development and Utilization, Hohhot 010018, China.

[d] Department of Sustainable Biomaterials, Virginia Polytechnic Institute and State University, Blacksburg, VA, 24060, USA.

*Corresponding author: Xiaotao Zhang, Email: lianzixiaotao@163.com; Ximing Wang, Email: wangximing@imau.edu.cn
† These authors contributed equally to this work.

Text S1

Characterization. The morphology and structure of the wood sponges were characterized by field emission scanning electron microscopy (Hitachi S4800, Japan) equipped with an energy dispersive X-ray spectroscopic detector for mapping. The high-resolution transmission electron microscopic (HRTEM) and selected area electron diffraction (SAED) images of the ZnO/ZnS@AWA were taken using a FEI HRTEM (FEI Tecnai G2, USA). The optical properties of the samples were studied by UV−vis absorption spectroscopy (Shimadzu UV-3600i Plus, Japan) and photoluminescence (PL) (Edinburgh FLS1000, England) spectroscopy at room temperature. The XRD patterns were obtained using a TD-3500 X-Ray Powder Diffractometer (Dandong Tongda Instrument Co., Ltd, China). X-ray photoelectron spectroscopy (XPS) (ESCALAB 250Xi, Thermo Fisher Scientific, USA) was performed with Al Kα X-rays as the excitation source. Total C, H, O and N contents of samples were determined using an elemental analyzer (Euro EA3000 Organic element analyzer, Italian). A Perkin Elmer L1600400 Spectrum TWO FT-IR was used to measure the FT-IR spectrum. Acid-insoluble lignin, hemicellulose and α-cellulose contents were measured in accordance with the GB/T 2677.8-94, GB/T 2677.10-1995 and GB/T 744-1989 standards, respectively. Carboxyl group content was measured using conductivity titration method. The nitrogen adsorption−desorption isotherms of samples were examined via JW-BK analyzer (Beijing JWGB SCI.&TECH, China). The electron paramagnetic resonance (EPR) signals of spin-trapped radicals were conducted on a EMXplus-6/1 spectrometer using spin-trap reagent 5,5-dimethyl-1-pyrroline-N-oxide (DMPO) in water for •OH and methanol for $•O_2^-$, (4-oxo-2,2,6,6-tetramethyl) TEMP for $1O_2$, respectively. A 500 W Hg lamp was used as the light source.

The photoelectrochemical properties were measured using a conventional three electrode electrochemical workstation (CHI750E, China) with the samples as the working electrode, an Ag/AgCl electrode as the reference electrode, and a Pt plate as the counter electrode,

respectively, with a 0.5 M Na2SO4 aqueous solution electrolyte. The film working electrodes were prepared by drop-casting samples, ethanol and Nafion suspensions onto FTO glass substrates followed by drying the film at room temperature. The photocurrent response curves were also recorded with xenon lamp light on and off (20s on and 20s off). Electrochemical impedance spectroscopy (EIS) was conducted using a potentiostatic method with a frequency from 0.1 kHz to 100 kHz. The Mott-Schottky plots were obtained at a constant frequency of 1.0 kHz and potential range -1-2V.
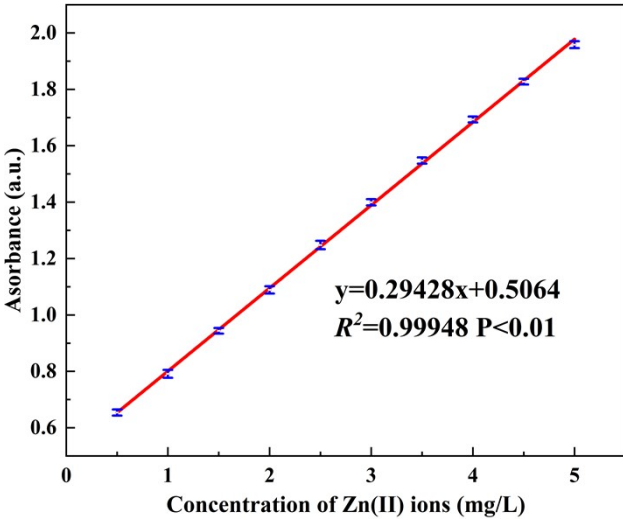
1.Supplementary Figures

$y=0.29428x+0.5064$
$R^2=0.99948$ P<0.01

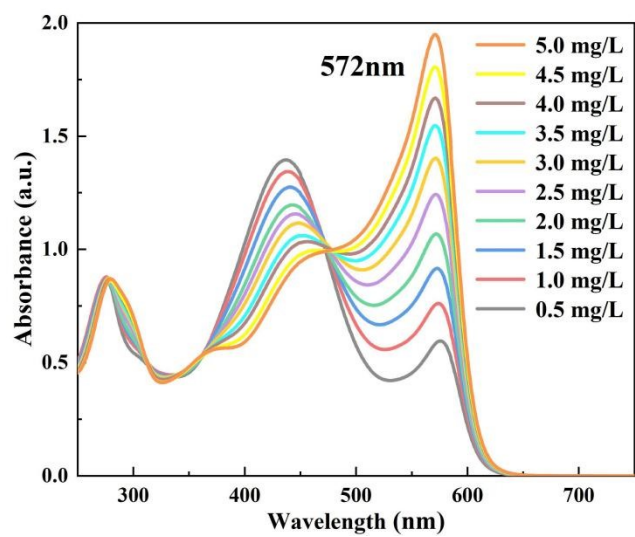**Fig. S1** The standard curve of Zn(II)

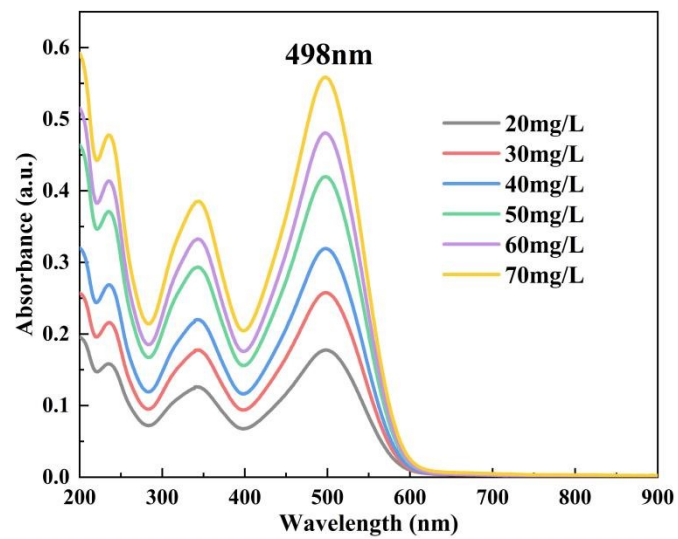**Fig. S2** The wavelength scan of different concentration of Zn(II).

Fig. S3 The wavelength scan of different concentration of Congo red
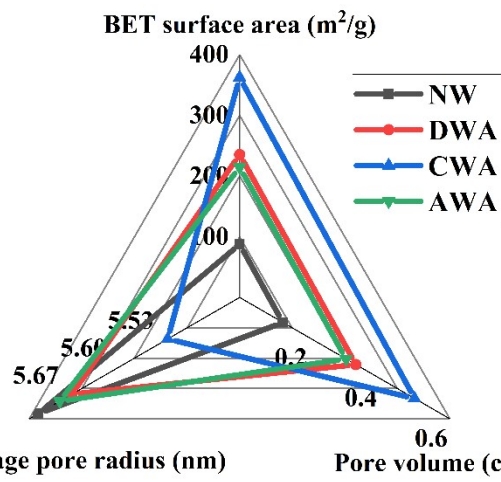
Fig. S4 The BET surface area, pore volume and average pore radius of NW, DWA, CWA and AWA.
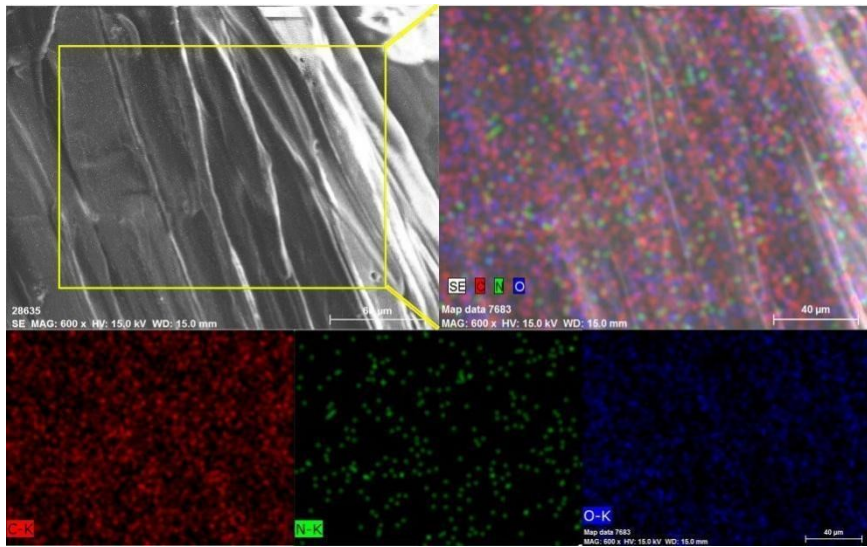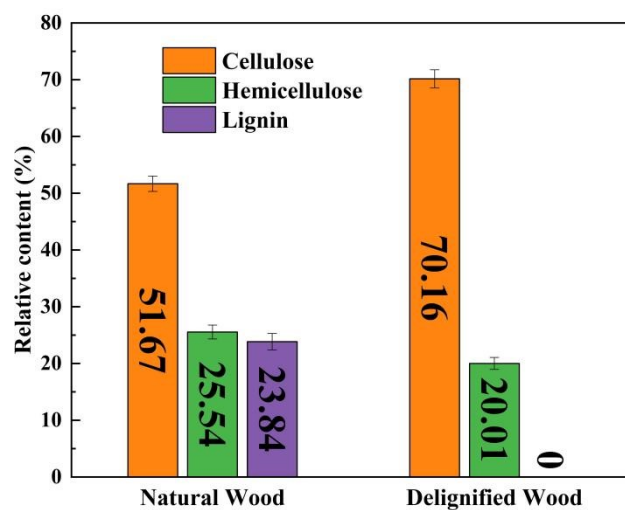
Fig. S5 EDX-mapping of AWA.

Fig. S6 Relative content of cellulose, hemicelluloses, and lignin in Natural Wood and Delignified Wood obtained from the chemical composition analysis.
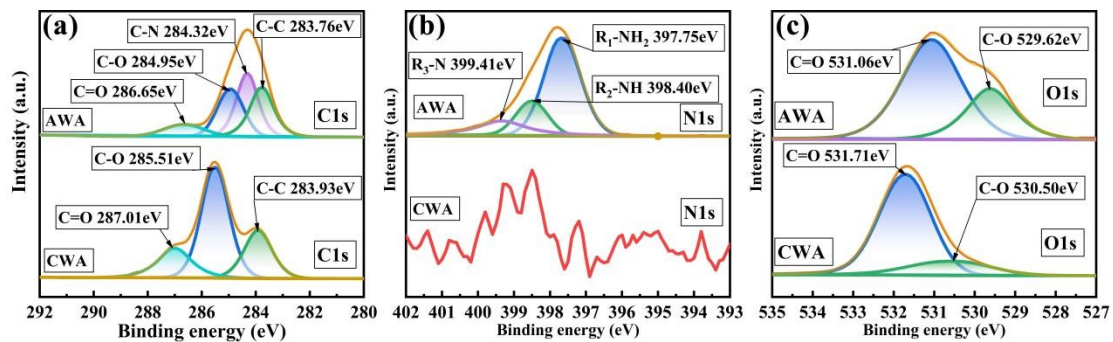
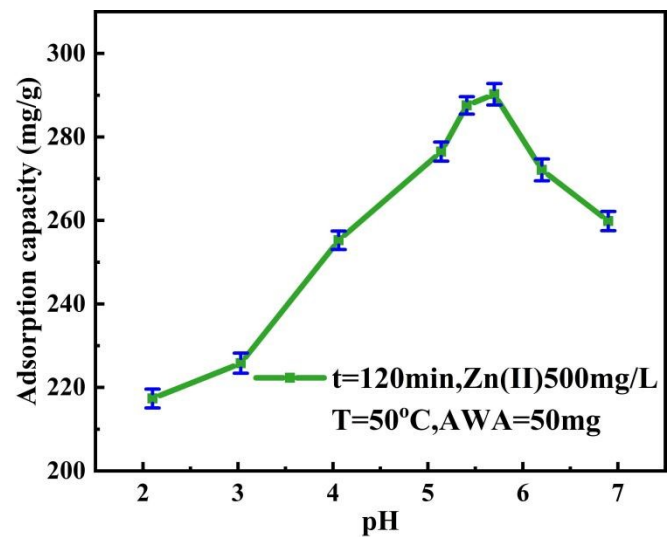**Fig. S7** XPS spectra of AWA and CWA: C1s peak (a), N1s peak (b) and O1s peak (c)

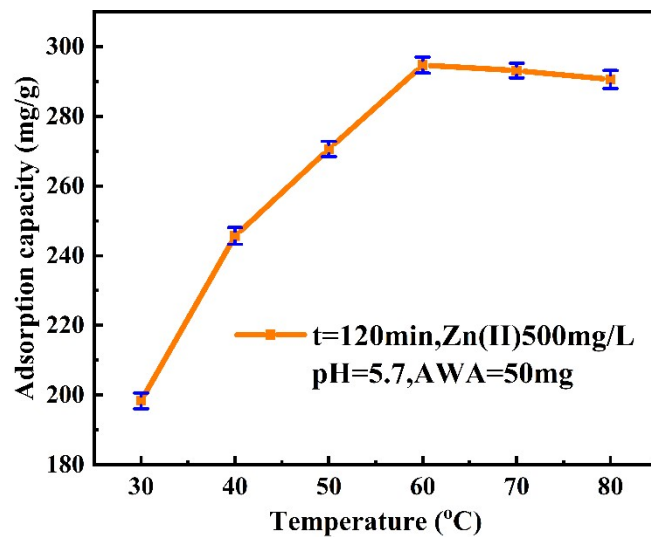**Fig. S8** Effect of solution pH on the adsorption capacity of AWA.

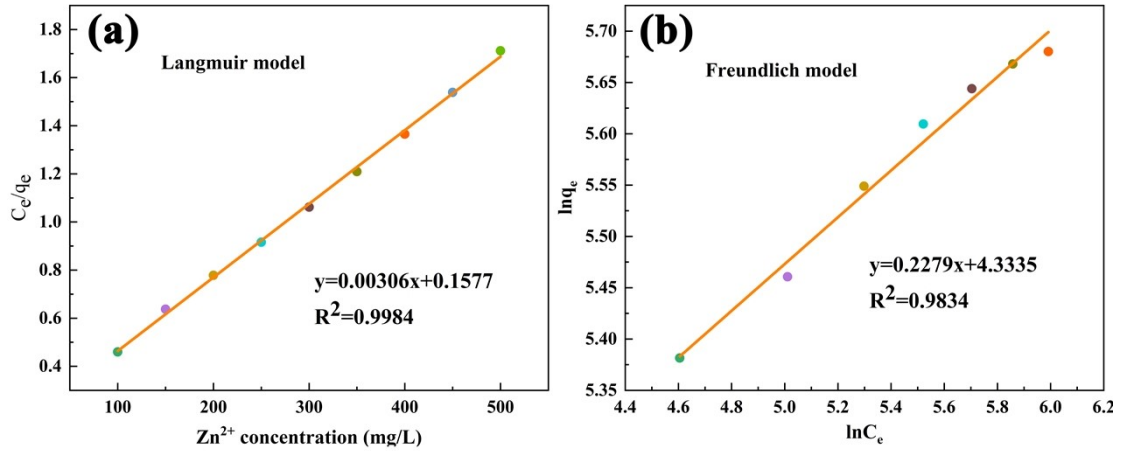**Fig. S9** Effect of temperature on the adsorption capacity of AWA.

Fig. S10 Adsorption isotherm linear fitting curves of Langmuir model and Freundlich model. Adsorption isotherm model equation as following shows.

Langmuir model:

$$\frac{C_e}{q_e} = \frac{1}{bq_m} + \frac{C_e}{q_{max}}$$

(1)

The essential characteristics of the Langmuir isotherm can be expressed by a dimensionless constant called the equilibrium parameter R_L, which is defned by the following equation (Eq. 2):

$$R_L = \frac{1}{1 + K_L C_0}$$

(2)

Freundlich model:

$$\ln q_e = \ln K_f + \frac{1}{n} C_e$$

(3)

where q_{max} (mg/g) is the monolayer saturation adsorption capacity; C_e (mg/L) is the concentration of metal ions at equilibrium; K_L (L/mg) is the Langmuir constant related to the adsorption capacity; the value of R_L indicates the nature of the isotherm as unfavorable ($R_L>1$), linear ($R_L=1$), favorable ($0<R_L<1$), or irreversible ($R_L=0$); K_f is the Freundlich constant, 1/n is the value used to indicate the heterogeneity of the interface; q_e (mg/g) is the adsorption capacity at equilibrium.
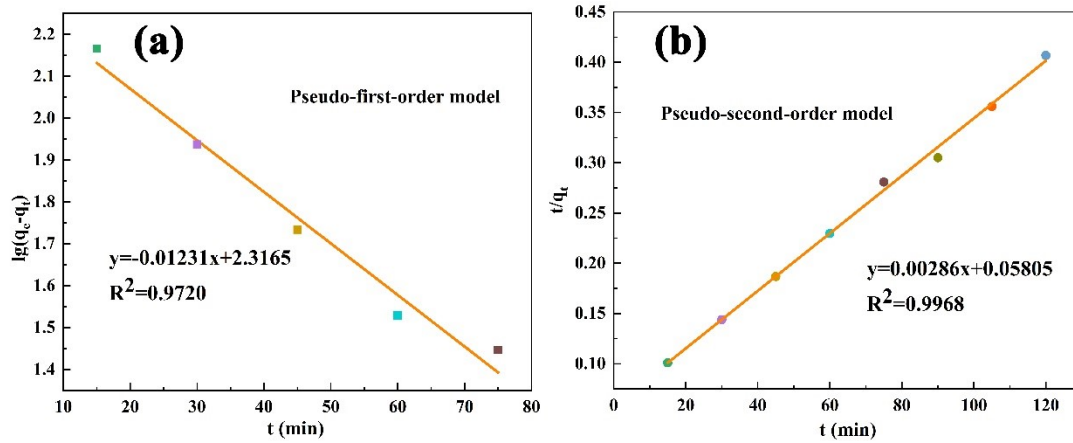
13

Fig. S11 Adsorption kinetics linear fitting curves of Pseudo-first-order model and Pseudo-second-order model.

Adsorption kinetics model equation as following shows.

Pseudo-frst-order model:

$$\log (q_e - q_t) = \log q_e - \frac{k_{1t}}{2.303} \tag{4}$$

Pseudo-second-order model:

$$\frac{t}{q_t} = \frac{1}{k_2 q_e^2} + \frac{t}{q_e} \tag{5}$$

where q_e and q_t are the amounts of heavy metal ions adsorbed (mg/g) at equilibrium and at time t (min), respectively; k_1 (min^{-1}) is the Pseudo-frst-order rate constant; k_2 [g·(mg/min)$^{-1}$] is the rate constant of the Pseudo-second-order adsorption kinetic equation.
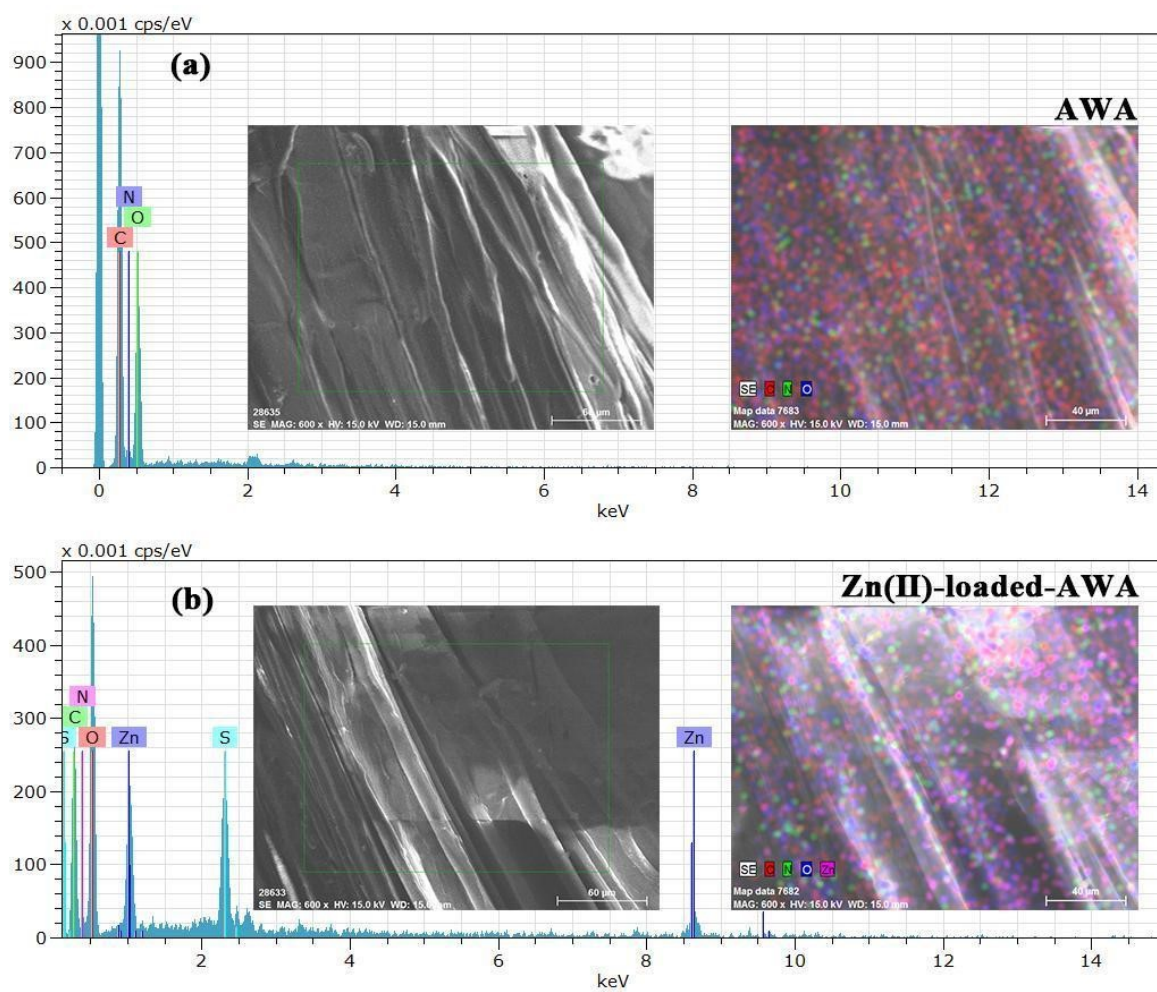
Fig. S12 EDX and element mapping of AWA (a) and Zn(II)-loaded-AWA(b).
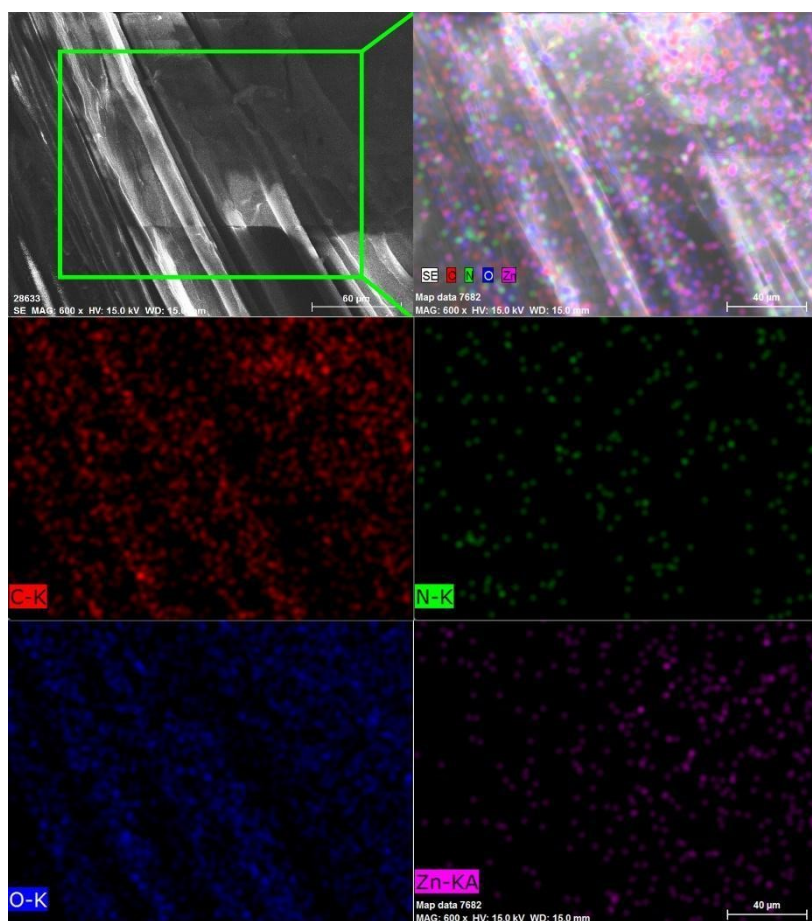
Fig. S13 EDX-mapping of Zn(II)-loaded-AWA.
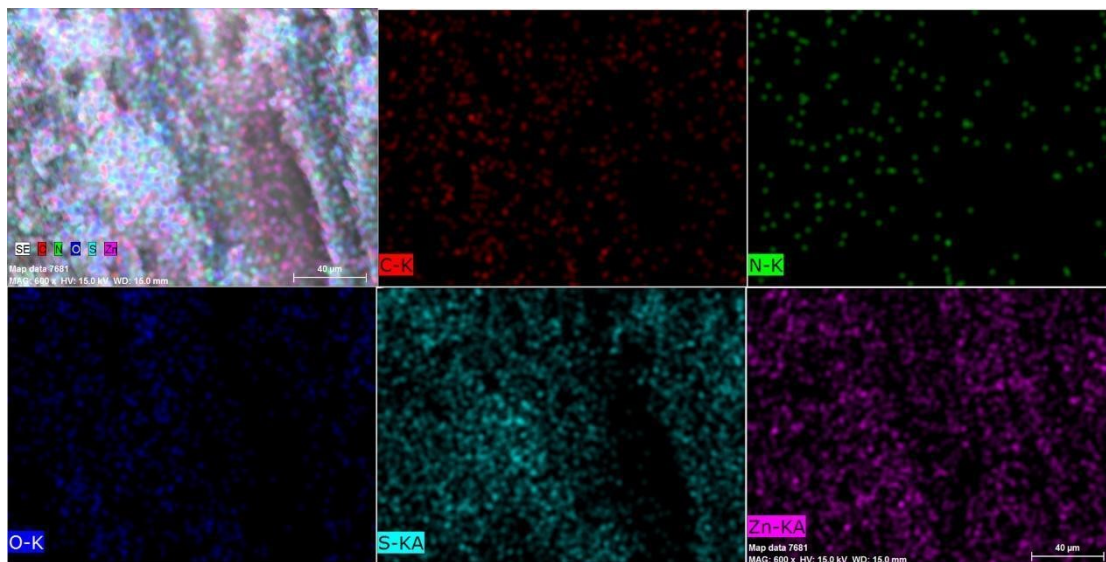
Fig. S14 EDX-mapping of ZnO/ZnS@AWA
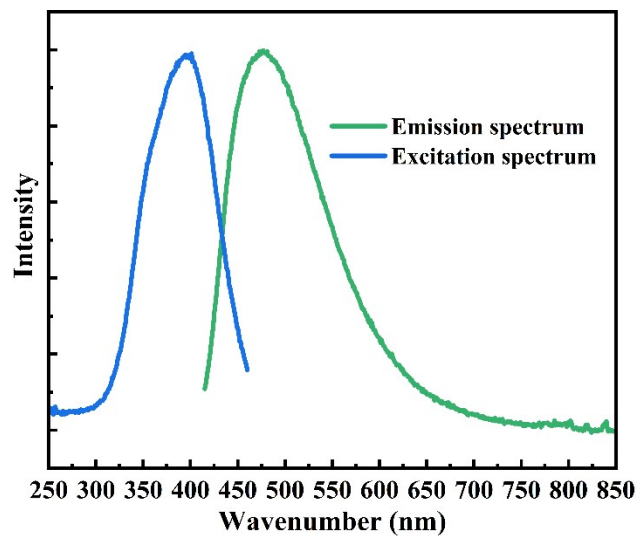
Fig. S15 Steady-state PL spectra of ZnO/ZnS@AWA (d)
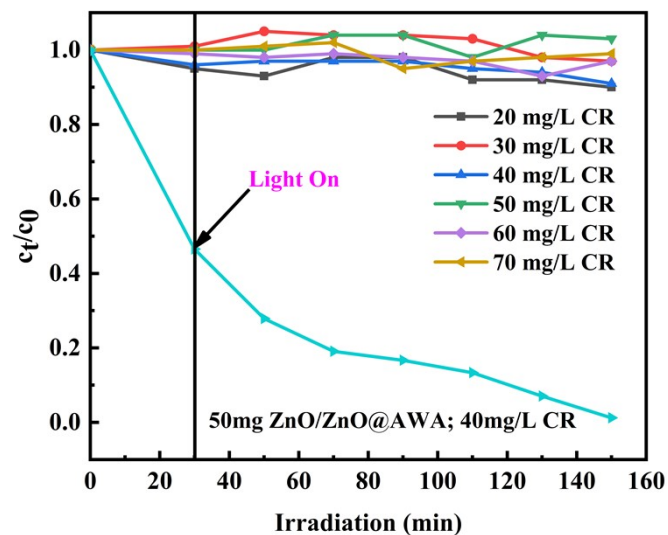
Fig. 16 Photocatalysis degradation experiment for CR under UV light without photocatalysts.
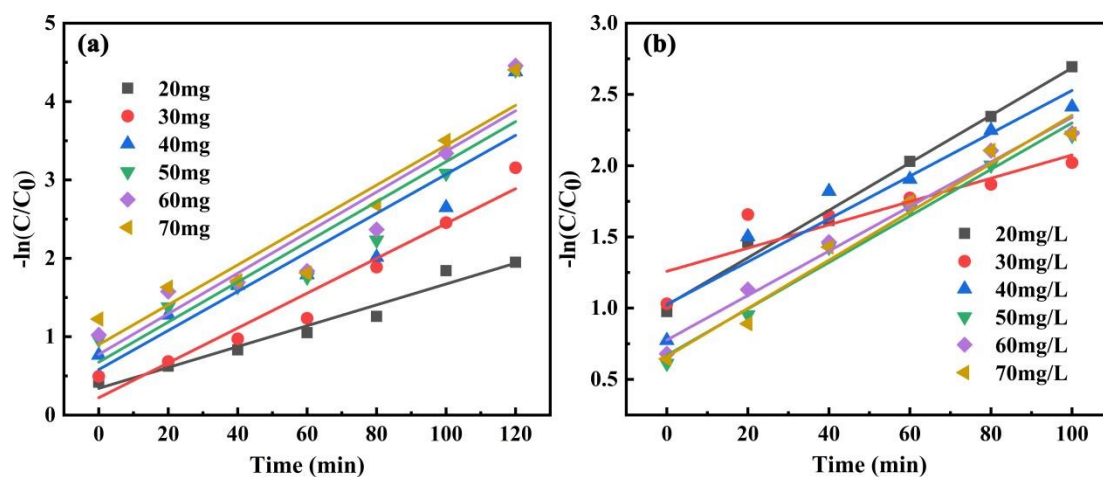
Fig. S17 Pseudo first-order kinetic fitting curves under ultraviolet-light irradiation of different amount of catalyst (a) and CR initial concentration(b).

L-H kinetics model equation as following shows.

Pseudo-frst-order kinetic model:

$$-\ln\left(\frac{A_t}{A_0}\right) = k_{app}t$$

(5)

where A_0 and A_t are the absorbance of the Congo red in 498nm at initial and at time t, respectively, k_{app} is the apparent reaction rate constant.
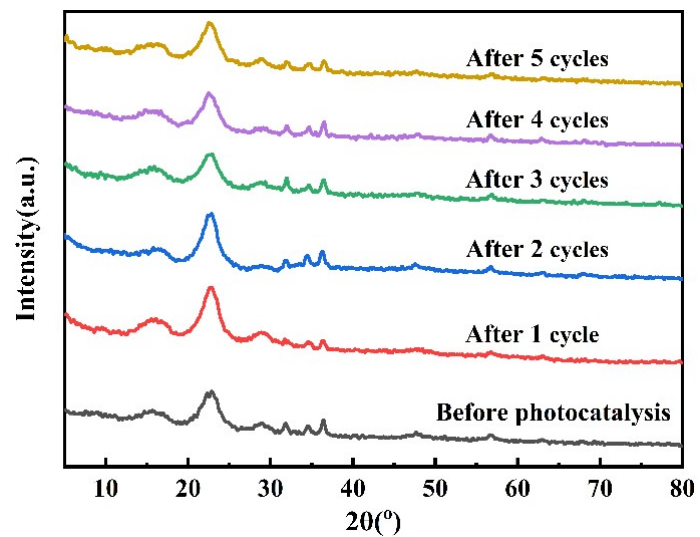
Fig. S18 XRD patterns of ZnO/ZnS@AWA before and after photocatalysis experiment
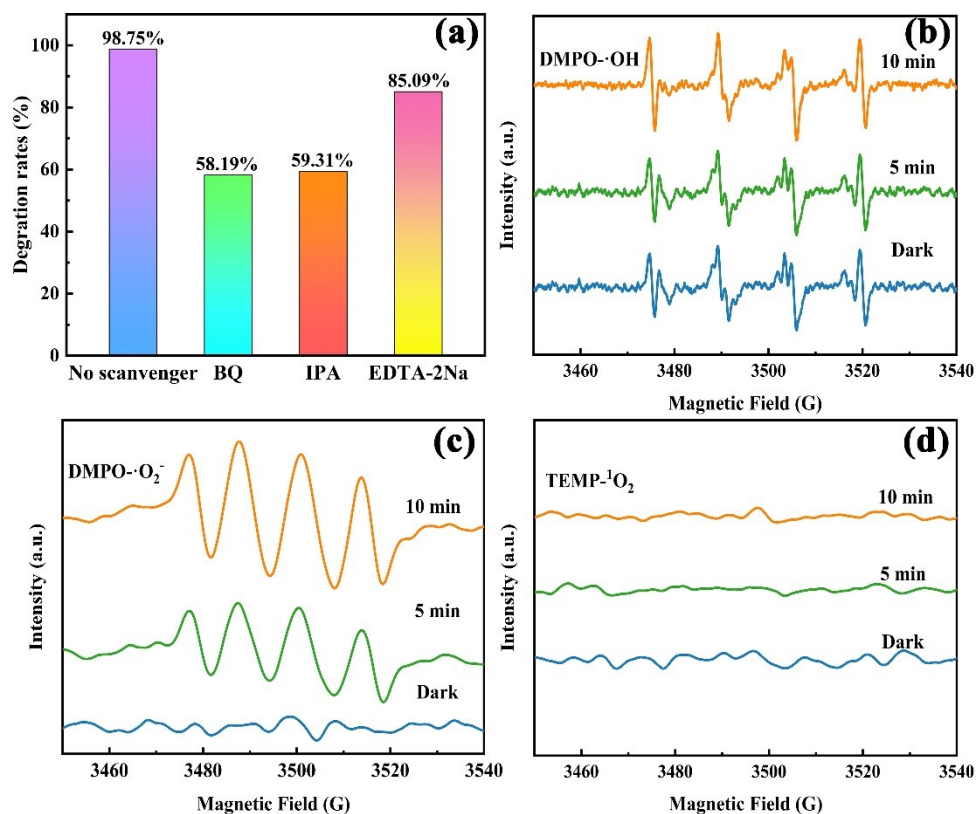
Fig. S19 Effect of different scavengers on ZnO/ZnS@AWA for the photodegradation of CR (a); EPR spectra of the ZnO/ZnS@AWA under UV-irradiation for DMPO-·OH(b), DMPO-·O_2^-(c) and TEMP-$^1O_2$(d).
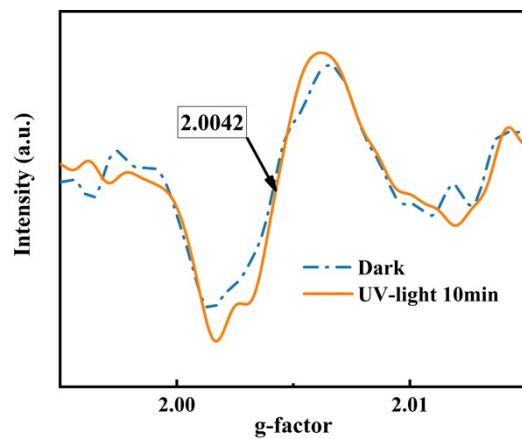
Fig. S20 EPR spectra of the ZnO/ZnS@AWA under dark and UV-light 10 min.

2. Supplementary Tables

Table. S1 Mean values of volume, weight and density of poplar wood (NW), Delignified@Wood-Aerogel (DWA), Carboxylation@Wood-Aerogel (CWA) and Amination@Wood-Aerogel (AWA).

Samples	Volume (cm³)	Weight (g)	Density (g·cm⁻³)
NW	3.375	1.642	0.487
DWA	3.825	0.949	0.248
CWA	5.175	0.506	0.156
AWA	6.750	0.938	0.139

Table. S2 Relative content of carboxyl group in CWA obtained from the conductivity titration method.

Samples	Time (h)	TEMPO (g)	NaClO$_2$ (g)	NaClO (mL)	Carboxyl Content (mmol/g)
1#	24	0.032	2.26	80	0.64
2#	24	0.064	4.52	80	0.72
3#	24	0.096	6.78	80	0.96
4#	24	0.128	9.04	80	1.013
5#	48	0.032	2.26	80	0.693
6#	48	0.064	4.52	80	0.747
7#	48	0.096	6.78	80	1.067
8#	48	0.128	9.04	80	1.174

Table. S3 R^2 and constant values for the different adsorption isotherm models of Zn(II) on AWA.

Metals	Parameters		Langmuir model		Freundlich model
Zn(II)	R^2		0.9984		0.9834
	Constants	K_L	0.0194 L/mg	K_f	76.214 L/g
		q_{max}	326.79 mg/g	$1/n$	0.228

Table. S4 R^2 and constant values for the different adsorption kinetics models of Zn(II) on AWA

Metals	Parameters	Pseudo-first-order model		Pseudo-second-order model	
Zn(II)	R^2		0.9720		0.9968
	Constants	k_1	0.02835 min^{-1}	k_1	0.00014g/(mg·min)
		q_e	207.25 mg/g	q_e	349.65mg/g

Table. S5 Comparison studies of the maximum monolayer adsorption of Zn(II) ions onto different adsorbent materials

Adsorbent	Adsorption capacity (mg/g)	Adsorption isotherm model	Adsorption kinetics model	Ref.
AWA	326.79	Langmuir	Pseudo second-order	This work
MgSi-HC	227.3	Sips	Pseudo second-order	[1]
Alkali-PEI-HC	207	Freundlich	Pseudo second-order	[2]
Titanate nanotubes	139.44	Langmuir	Pseudo second-order	[3]
MCC-g-polyIL	122.78	Freundlich	Pseudo second-order	[4]
Sandwich-like Nanofibrous Mats	104.31	Langmuir	Pseudo second-order	[5]
Green alga Neochloris oleoabundans	59.50	Langmuir	Pseudo second-order	[6]
Pinus elliottii sawdust	16.55	Langmuir	Pseudo second-order	[7]

Table. S6 Comparison studies of the degradation of Congo red onto different adsorbent materials

Photocatalyst	Concentration (mg/L)	Time (min)	Degradation Rate	Ref.
ZnO/ZnS@AWA	40	120	98.84%	This work
ZnCCSs	50	120	96.53	[8]
Bi_2S_3	35	150	98%	[9]
Cu/TiM	25	210	98%	[10]
ZIF-8@TiO_2 (5%KI)	20	40	97%	[11]
Pd/ZnO	16	60	98.2%	[12]
ZnO/SnO_2	5	120	88.14%	[13]

Reference

1. J. Deng, X. Li, X. Wei, Y. Liu, J. Liang, B. Song, Y. Shao and W. Huang, *Chemical Engineering Journal*, 2020, **387**.
2. X. He, T. Zhang, Q. Xue, Y. Zhou, H. Wang, N. S. Bolan, R. Jiang and D. C. W. Tsang, *Sci Total Environ*, 2021, **778**, 146116.
3. W. Linghu, Y. Sun, H. Yang, K. Chang, G. Sheng, T. Hayat, N. S. Alharbi and J. Ma, *Journal of Molecular Liquids*, 2017, **244**, 146-153.
4. A. Wang, S. Li, H. Chen, Y. Hu and X. Peng, *Cellulose*, 2019, **26**, 6849-6859.
5. Y. Wu, X. Qiu, S. Cao, J. Chen, X. Shi, Y. Du and H. Deng, *J Colloid Interface Sci*, 2019, **539**, 533-544.
6. S. Gu and C. Q. Lan, *J Hazard Mater*, 2021, **418**, 126336.
7. J. Bortoluz, A. Cemin, L. R. Bonetto, F. Ferrarini, V. I. Esteves and M. Giovanela, *Cellulose*, 2019, **26**, 4895-4908.
8. J. You, C. Liu, X. Feng, B. Lu, L. Xia and X. Zhuang, *Carbohydrate Polymers*, 2022, **288**.
9. C. Sambathkumar, V. Manirathinam, A. Manikandan, M. Krishna Kumar, S. Sudhahar and P. Devendran, *Journal of Materials Science: Materials in Electronics*, 2021, **32**, 20827-20843.
10. U. Arellano, J. A. Wang, L. F. Chen, M. Asomoza, A. Guzmán, S. Solís, A. Estrella, S. Cipagauta and L. E. Noreña, *Catalysis Today*, 2020, **349**, 128-140.
11. Z. Liu, W. Zhang, X. Zhao, X. Sheng, Z. Hu, Q. Wang, Z. Chen, S. Wang, X. Zhang and X. Wang, *Materials*, 2022, **15**.
12. C. B. Ong, A. W. Mohammad, R. Rohani, M. M. Ba-Abbad and N. H. H. Hairom, *Process Safety and Environmental Protection*, 2016, **104**, 549-557.
13. M. H. Sayadi, S. Ghollasimood, N. Ahmadpour and S. Homaeigohar, *Journal of Photochemistry and Photobiology A: Chemistry*, 2022, **425**.